



Prediction of NbTaTiZr-based high-entropy alloys with high strength or ductility: First-principles calculations

Yanan Wu^a, Yun Zhang^b, Ze Li^a, Zhiyu Liu^a, Erjun Zhao^{c, **}, Jingshun Liu^{a,*}

^a School of Materials Science and Engineering, Inner Mongolia University of Technology, Hohhot, 010051, PR China

^b Faculty of Instrumentation, Belarusian National Technical University, Minsk, 220013, Belarus

^c College of Sciences, Inner Mongolia University of Technology, Hohhot, 010051, PR China



ARTICLE INFO

Keywords:

Refractory high-entropy alloys (RHEAs)

First-principles calculations

Mechanical properties

Phase structure

Electronic performance

ABSTRACT

Refractory high-entropy alloys (RHEAs) have a great potential in high-temperature electronics, extensive aerospace and biomedical applications due to their unique strength and ductility. Herein, the effects of alloying elements on the mechanical and electronic properties of NbTaTiZrX (X = V, Mo, Hf, W and Re) RHEAs are investigated by using the density functional theory (DFT) in combination with the special quasi-random structure (SQS) and virtual crystal approximation (VCA) methods. The calculated results show that alloying of Mo, W and Re with high elastic modulus can enhance the strength and the hardness of RHEAs. Among them, NbTaTiZrRe RHEA with the best strengthening effect has a yield strength of exceeds 2 GPa, which is notably higher than other considered high-entropy alloys. For alloying of V and Hf, the ductility of RHEAs is improved, and among which, NbTaTiZrHf RHEA has a relatively best ductility. Compared with other NbTaTiZrX RHEAs, spiral dislocations in NbTaTiZrHf RHEA are more prone to nucleate, and which confirms its excellent ductility. Moreover, the reduction of pseudo energy gaps and the formation of Hf–Hf strong metallic bonds further confirm its metallic ductility from the electronic density of states and charge density. The theoretical predictions in this study are congruent with the existing experimental data, and have certain theoretical guidance relevance for enhancing the mechanical characteristics of NbTaTiZrX (X = V, Mo, Hf, W and Re) RHEAs.

1. Introduction

High-entropy alloys (HEAs) are unique materials and typically composed of at least five metallic elements with equal or essentially equal atomic weights [1]. The special composition ratio provides a wide range of opportunities for the design of alloy materials. Moreover, the excellent properties of HEAs such as high strength, high plasticity, and corrosion resistance have greatly expanding their application range [2]. Particularly, refractory high-entropy alloys (RHEAs) consisting of elements like Nb, Ta, Ti, and Zr exhibit excellent mechanical properties in high-temperature applications and show great potential in biomedical applications, such as orthopedic implants [3]. In 2010, WN₆Mo₂Ta and WN₆Mo₂TaV firstly introduced and exhibited good high-temperature stability compared to Inconel718 nickel-based superalloys [4]. RHEAs such as HfNbTaTiZr [5], HfMoTaTiZr and HfMoNbTaTiZr [6] in equimolar ratios, as well as non-equimolar ratios of Zr₄₅Ti₁₅Nb₃₀Ta₁₀ [7], Ti₃₀Zr₃₀Hf₁₆Nb₂₄ [8] and Ti₃₀Ni₃₀Fe₁₀Hf₁₀Nb₂₀ [9] are promising

materials with the potential for extensive aerospace applications due to their superior properties, including high strength, remarkable tensile ductility, and excellent high-temperature performance. Additionally, through the research on the structure, mechanical properties, and corrosion properties of TiZrHfNb [10], TiZrNbTa [11], MoNbHfZrTi [12], TiNbTaZrMo [13], TiZrHfNbTa [14], and HfMoNbTaTiZr [6], it is found that their performances are superior to other commercial bio-alloys like Ti6Al–4V. This strongly supports the application of RHEA in the biological field [3]. Due to the high melting point and difficulty in experimental preparation for RHEAs, it is inefficient by using traditional trial and error methods to design new RHEAs. Fortunately, theoretical arithmetic can be employed to rapidly and systematically explore the composition space, identify potential alloy components, and guide experimental design, thus accelerate the RHEAs development. In 2021, Bhandari et al. [15] investigated the structure, mechanical and thermodynamic properties of HfNbTaTiZr and Hf_{0.5}Nb_{0.5}Ta_{0.5}Ti_{1.5}Zr through first-principles calculations in combined with a special

* Corresponding author.

** Corresponding author.

E-mail addresses: ejzhao@imut.edu.cn (E. Zhao), jingshun_liu@163.com (J. Liu).

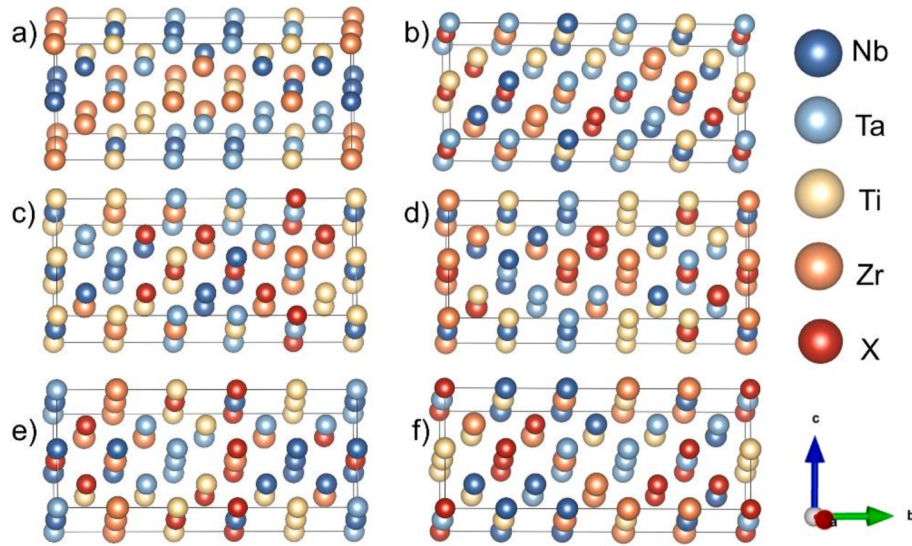


Fig. 1. NbTaTiZrX RHEAs with BCC structure constructed by SQS method.

a) NbTaTiZr; b) NbTaTiZrV; c) NbTaTiZrMo; d) NbTaTiZrHf; e) NbTaTiZrW; f) NbTaTiZrRe.

quasi-random structure (SQS) method, and also found that the calculated lattice constants, density, Young modulus, and Vickers hardness are consistent with the current experimental results, and which confirms that the SQS method is reasonable. Gao et al. [16] established a BCC solid solution structural model by using the virtual crystal approximation (VCA) method and determined the effects of Cr and Ti content on the structure, elastic properties and anisotropy of the VMoNbTaWM_x ($M = \text{Cr}, \text{Ti}$) RHEAs phase with BCC structure. Compared with the SQS method, the VCA method ignores the influence of the local environment on the system and is suitable for systems with similar chemical elements, and its calculation efficiency is superior to the SQS method [17].

This study utilizes four commonly used elements in RHEAs, namely Nb, Ta, Ti, and Zr, and incorporates a novel element X into NbTaTiZr-based RHEA in equal proportion. The relationship between the elastic constant, elastic modulus, hardness, strength, and plasticity of NbTaTiZrX RHEAs with elements is systematically analyzed both by SQS and VCA methods, and the influence of element alloying on its mechanical properties is revealed through electronic density of states and charge density, providing the theoretical guidance for the design of high-performance RHEAs and also accelerating the exploration and application of new RHEAs.

2. Calculation details

The SQS [18] method was generally adopted to generate the chemical disorder in RHEAs. For the SQS structure, multiple $2 \times 2 \times 5$ super monoliths with a fixed unit cell of 40 atoms were generated using the Alloy Theoretic Automated Toolkit (ATAT) algorithm [19,20], and the optimized total free energies and lattice constants of multiple cells of the same RHEA were compared, and those with lower energies and close to the experimental values of lattice constants were selected for the mechanical property calculations, the specific structures are shown in Fig. 1 a) - f). Moreover, the calculation results of the VCA method [21] were expanded in supporting information.

The VASP package [22] in the frame of DFT [23] was used to carry out the first-principles calculations of RHEAs. The generalized gradient approximation (GGA) [24] of Perdew-Burke-Ernzerhof (PBE) was selected as the exchange-correlation functional for electron interactions, and the electron-ion interactions are handled by the projector-augmented-wave [25] (PAW) approach. The plane-wave cutoff energy was set to 450 eV, and the Monkhorst-Pack technique with a $7 \times 7 \times 2$ k-points mesh was used to sample the Brillouin zone. The

Table 1

Common parameters of NbTaTiZrX ($X = \text{V, Mo, Hf, W, and Re}$) RHEAs.

RHEAs	T_m (K)	ΔS_{mix} J/(K·mol)	ΔH_{mix} KJ/mol	δ (%)	Ω	VEC
NbTaTiZr	2527.25	11.57	2.50	4.37	11.69	4.50
NbTaTiZrV	2450.20	13.48	0.32	5.77	103.24	4.60
NbTaTiZrMo	2601.00	13.45	-1.76	5.33	19.87	4.80
NbTaTiZrHf	2523.00	13.49	2.72	5.13	12.51	4.40
NbTaTiZrW	2751.20	13.44	-3.20	4.79	11.55	4.80
NbTaTiZrRe	2725.00	13.46	-4.80	4.63	7.64	5.00

maximum tolerance for the total energy and Hellman Feynman forces on all atoms was within 10^{-4} eV and 10^{-2} eV/Å, respectively. The elastic constant of NbTaTiZrX RHEAs was calculated using the energy-strain method [26] (formula S2).

3. Results and discussion

3.1. Structural analysis

To investigate the alloying effect of NbTaTiZr RHEA, the appropriate X elements are selected to fabricate NbTaTiZrX-based RHEAs. The evaluation criteria for element X are as follows: (1) X is a non-radioactive metal element; (2) To avoid combustion during the alloy formation, the boiling point of element X should be higher than the melting points of components of Nb, Ta, Ti and Zr; (3) The alloyed compounds should meet the criteria for HEAs, i.e. $-15 \text{ kJ/mol} \leq \Delta H_{\text{mix}} \leq 5 \text{ kJ/mol}$, $12 \text{ J/(K·mol)} \leq \Delta S_{\text{mix}} \leq 17.5 \text{ J/(K·mol)}$, $\delta < 6.5\%$, and $\Omega \geq 1.1$ [27,28]. The screening results are shown in Table S1, and the common parameters of the eligible RHEAs are listed in Table 1. Worthfully, all the considered RHEAs series that meet the above conditions are currently the most studied ones. Common properties of the elements selected for RHEAs are shown in Table S2. According to the Valence electron concentration (VEC) phase structure criterion proposed by Guo et al. [29], it is found that the VEC of NbTaTiZrX RHEAs is ≤ 6.87 , while indicating that they are all the BCC phases.

The relationship between energy and volume is calculated near the equilibrium volume to optimize the crystal structure of NbTaTiZrX RHEAs and used to estimate the ground-state properties (Fig. S2). The calculated XRD (Fig. S3) of the optimized structure was in agreement

Table 2

Lattice constants (\AA) of NbTaTiZrX (X = V, Mo, Hf, W, and Re) RHEAs.

RHEAs	a^{EXE}	a^{Vegard}	a^{SQS}	a^{VCA}
NbTaTiZr	3.368 [11]	3.378	3.362	3.392
NbTaTiZrV	3.327 [31]	3.363	3.292	3.334
NbTaTiZrMo	3.332 [31]	3.332	3.310	3.325
NbTaTiZrHf	3.406 [34]	3.411	3.396	3.424
NbTaTiZrW	3.325 [31]	3.335	3.312	3.332
NbTaTiZrRe	—	3.492	3.297	3.289

Table 3

Elastic constants (GPa) of NbTaTiZrX (X = V, Mo, Hf, W, and Re) RHEAs.

RHEAs	Methods	C_{11}	C_{12}	C_{44}	$C_{11} - C_{12}$	$C_{12} - C_{44}$
NbTaTiZr	SQS	170.19	113.03	38.10	57.15	74.94
	VCA	155.24	128.62	43.24	26.63	85.38
NbTaTiZrV	SQS	180.29	117.06	31.32	63.24	85.74
	VCA	165.31	146.77	55.81	18.54	90.95
NbTaTiZrMo	SQS	217.58	118.22	38.91	99.37	79.31
	VCA	212.10	136.54	41.85	75.56	94.69
NbTaTiZrHf	SQS	151.80	103.75	30.12	48.06	73.62
	VCA	133.71	125.08	39.01	8.635	86.07
NbTaTiZrW	SQS	212.70	126.66	43.07	86.04	83.59
	VCA	212.53	144.53	55.67	68.00	88.86
NbTaTiZrRe	SQS	237.55	114.86	54.27	122.69	60.59
	VCA	257.74	149.45	64.29	108.30	85.15

with the experiment results [11,30–32], confirming the rationality of the structure. Table 2 shows the lattice constants of NbTaTiZrX RHEAs. The volumes and lattice constants of the alloys changed with the size of the atomic radius. It is well known that the atomic radius gradually increases with the increase of atomic number in the same main group, hence the NbTaTiZrHf has the largest equilibrium volume and lattice constant; while the atomic radius gradually decreases with the increase of atomic number in the same periodic, so the NbTaTiZrRe has the smallest equilibrium volume and lattice constant. According to the Vegard law [33], the average lattice constant a^{Vegard} of NbTaTiZrX RHEAs was calculated. From Table 2, the a^{Vegard} is slightly larger than the experimental value a^{EXE} , while the optimized equilibrium lattice constant a^{SQS} is a little bit smaller than a^{EXE} . The above difference may be attributed to the fact that the experimental measurement of a^{EXE} is conducted at room temperature, a^{Vegard} is the average lattice constant of elements at high temperatures, and a^{SQS} corresponds to a value at 0 K. As temperature increases, the lattice slightly expands, which is in line with the rationale of the calculations. Meanwhile, the total energy as a function of the corresponding volume also demonstrates the phase stability of these RHEAs. The VCA method exhibits a certain level of accuracy in calculating similar elements. After optimization of the VCA method, a^{VCA} is extremely near to a^{SQS} , indicating the suitability of the VCA method for producing RHEAs. The optimized lattice constant of NbTaTiZrRe RHEA is significantly smaller than a^{Vegard} , but a^{SQS} and a^{VCA} are very similar. For NbTaTiZrRe RHEA, the calculated results can serve for future research.

3.2. Mechanical property analysis and discussion

Elastic constants of a type material determine its elastic properties and affect its mechanical properties. Table 3 lists the elastic constants of NbTaTiZrX RHEAs calculated by the SQS and VCA methods. The predicted NbTaTiZrX RHEAs have satisfied the mechanical stability criterion of cubic crystal structure: $C_{11} > |C_{12}|$, $C_{44} > 0$, $C_{11} + 2C_{12} > 0$ [16]. For alloying of Mo, W and Re, it is interesting to note that the elastic constant of RHEAs increases with the increase of atomic number. But for Hf-alloying, its elastic constants significantly reduce, indicating that NbTaTiZrHf RHEA has lower resistance to external forces than other RHEAs. Furthermore, the experiment revealed that Hf-alloying can reduce RHEA strength, while alloying of Mo and W can enhance RHEAs

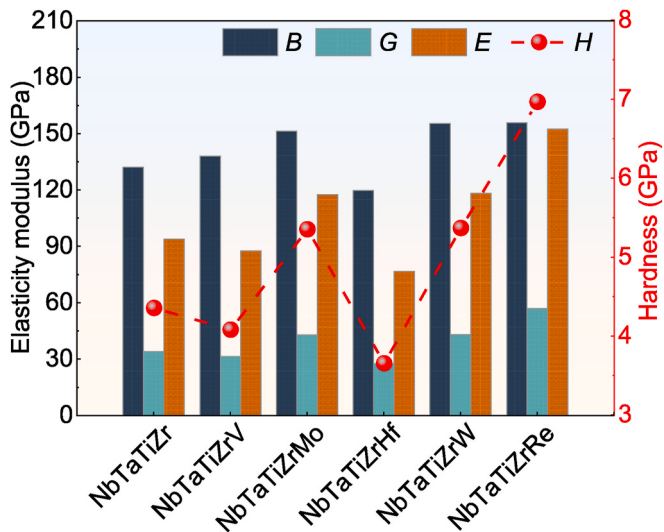


Fig. 2. Bulk modulus, Shear modulus, Young modulus, and hardness of NbTaTiZrX (X = V, Mo, Hf, W, and Re) RHEAs calculated by SQS method.

strength [5,31,35]. Cauchy pressure can indicate material atomic bonding qualities and ductility, and $C_{12} - C_{44} > 0$ suggests metallic bonding [36]. For NbTaTiZrX RHEAs, their Cauchy pressure values are all greater than zero, predicting the presence of metallic bonding in RHEAs with certain ductility. Among them, the Cauchy pressure value for Re-alloying is markedly reduced, indicating that the ductility of NbTaTiZrRe RHEA is worse than other RHEAs.

Elastic modulus is a crucial physical property that determines an object's ability to resist material deformation when subjected to stress. It is primarily characterized by three parameters: bulk modulus B , shear modulus G , and Young modulus E , which represent the alloy's resistance to bulk, shear, and elastic deformation, respectively. The higher elastic modulus corresponds to a greater deformation resistance [37]. Fig. 2 shows the bulk modulus, shear modulus, Young modulus, and hardness of NbTaTiZrX RHEAs calculated by SQS methods. The moduli of these materials were calculated by Voigt Reuss Hill approximation [38]. As can be seen from Fig. 2, alloying of Mo, W and Re for RHEAs can significantly increase their elastic modulus values, thereby enhancing their resistance to deformation. Among those alloying elements, Re-alloying has the most pronounced strengthening effect, while Hf-alloying drastically reduces the deformation resistance of RHEA. The experimental and calculated results also exhibit consistency. For example, the calculated E value of NbTaTiZr RHEA is approximately 94 GPa, and experimental measurements typically range from 80 to 116 GPa [30,39,40]. For NbTaTiZrHf RHEA, the calculated E value is approximately 77 GPa, and the range of experimental measurements is 59–85 GPa [34,38]. According to Table S2, when multiple alloying elements are mixed in a nearly equal atomic ratio to form a single-phase solid solution structure, the lattice structure of RHEs inevitably undergoes distortion due to differences in atomic radii between the constituent atoms and mismatches in physical properties such as elastic modulus. After the addition of X, the trend of elastic modulus change of NbTaTiZrX RHEAs is consistent with the trend of elastic modulus value change of element X. For example, adding elements such as W and Re with larger bulk modulus and Young's modulus results in higher B and E values for RHEA, while adding elements such as Hf and V with smaller shear modulus results in lower G values. Re has the largest elastic modulus, and the addition of it to the NbTaTiZr RHEA makes NbTaTiZrRe possess a larger elastic modulus than the other RHEAs. And lattice distortion can reduce the elastic modulus of materials [41], so adding Hf elements with the maximum radius results in RHEA having the smallest elastic modulus. Additionally, as shown in formula (1), based on the hardness formula proposed by Zhao et al. [42] to evaluate

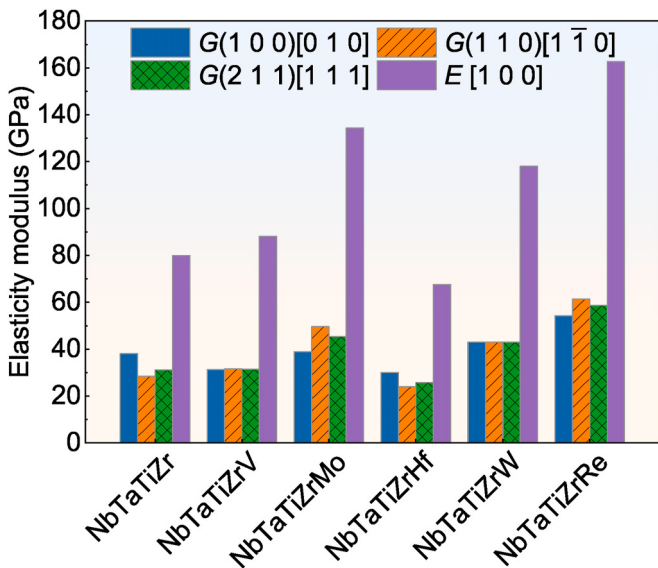


Fig. 3. Elastic modulus in different directions of NbTaTiZrX ($X = V, Mo, Hf, W$, and Re) RHEAs calculated by SQS method.

the material's resistance to deformation, and the calculation curve is shown in Fig. 2.

$$H_v = 0.79 + 0.10G + 1.47 \times 10^{-4}G^2 \quad (1)$$

From Fig. 2, the growth trend of H_v is consistent with Young modulus and shear modulus. Among them, Hf-alloying observably reduces the theoretical hardness of RHEA, and the predicted H_v is 3.6 GPa, which agrees with the experimental results of 359 HV [30]. Alloying of Mo, W and Re significantly increases their theoretical hardness, which agrees with experimental values for NbTaTiZrMo and NbTaTiZrW [31,35]. Among these elements, Re-alloying shows the highest hardness value of 7.03 GPa.

In order to further evaluate the deformation resistance of NbTaTiZrX RHEAs, the elastic modulus in different crystallographic directions were calculated, including the shear modulus in the $(1\ 0\ 0)$ $[0\ 1\ 0]$, $(1\ 1\ 0)$ $[1\ \bar{1}\ 0]$, $(2\ 1\ 1)$ $[1\ 1\ 1]$ directions, and the Young modulus in the $[1\ 0\ 0]$ direction. Those values reflect the ability to resist shear deformation along the $(1\ 0\ 0)$ $[0\ 1\ 0]$, $(1\ 1\ 0)$ $[1\ \bar{1}\ 0]$ and $(2\ 1\ 1)$ $[1\ 1\ 1]$ directions, as well as the ability to resist elastic deformation along the $[1\ 0\ 0]$ direction. Herein [43] :

$$G_{(1\ 0\ 0)[0\ 1\ 0]} = C_{44} \quad (2)$$

$$G_{(1\ 1\ 0)[1\ \bar{1}\ 0]} = \frac{C_{11} - C_{12}}{2} \quad (3)$$

$$G_{(2\ 1\ 1)[1\ 1\ 1]} = \frac{3C_{44}(C_{11} - C_{12})}{C_{11} - C_{12} + 4C_{44}} \quad (4)$$

$$E_{[1\ 0\ 0]} = (C_{11} - C_{12}) \left(1 + \frac{C_{12}}{C_{11} + C_{12}} \right) \quad (5)$$

Fig. 3 presents the elastic modulus calculated by SQS methods in different directions of NbTaTiZrX RHEAs. It can be seen that the shear modulus of RHEAs various in different directions, indicating that they are anisotropy. From Fig. 3, it is interesting to note that the alloying of Mo, W and Re significantly enhance the resistance of RHEAs to material deformation in all the directions. On the contrary, Hf-alloying greatly reduces the resistance of RHEA to material deformation in different directions. Comparing Fig. 3 and S5, it can be found that the elastic modulus calculated by the SQS method in different directions are higher than those calculated with VCA method. This may be due to the fact that the SQS method considers the influence of atomic position changes,

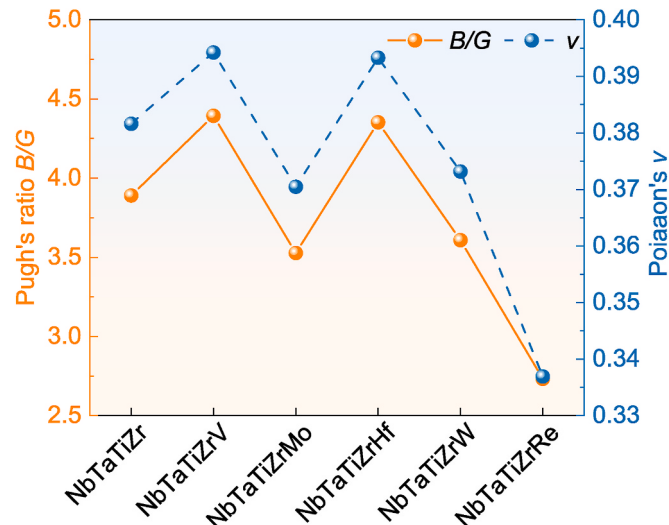


Fig. 4. Pugh's ratio and Poisson's ratio of NbTaTiZrX ($X = V, Mo, Hf, W$, and Re) RHEAs calculated by SQS method.

Table 4

Yield strength (GPa) of NbTaTiZrX ($X = V, Mo, Hf, W$, and Re) RHEAs.

RHEAs	σ_y^{SQS}	σ_y^{VCA}	σ_y^{EXE}
NbTaTiZr	1.45	1.20	1.02 [39]
NbTaTiZrV	1.36	1.23	–
NbTaTiZrMo	1.78	1.68	1.39 [35]
NbTaTiZrHf	1.21	0.85	1.02 [34]
NbTaTiZrW	1.79	1.89	–
NbTaTiZrRe	2.32	2.44	–

while the VCA method provides values closer to the directional average. Meanwhile, there is a significant difference in the elastic modulus in different directions of NbTaTiZrV RHEA calculated by the two methods. Comparing Fig. 1 b), it is found that there is no V atom in the $(1\ 0\ 0)$ plane of the NbTaTiZrV RHEA structure. Which indicates that the deformation resistance of NbTaTiZrV RHEA is more influenced by the atomic position.

Both brittleness and ductility of metallic materials are very important parameters for evaluating the strength of materials, which is commonly determined by Poisson's ratio v or Pugh's ratio (the ratio of bulk modulus to shear modulus, B/G). Typically, materials with $v > 0.26$ or $B/G > 1.75$ are ductile, whereas they are brittle. Increasing v and B/G values enhances the ductility of the alloy [44,45]. Fig. 4 displays the Pugh's ratio and Poisson's ratio of NbTaTiZrX RHEAs calculated by SQS method. It can be seen that the v values of all the predicted RHEAs are greater than 0.26, and the B/G values are greater than 1.75, indicating that NbTaTiZrX RHEAs are all the ductile materials. The alloying of Hf and V can enhance RHEAs ductility, while alloying of Mo, W, and Re can decrease RHEAs ductility, with NbTaTiZrRe displaying the lowest ductility. This agrees with experimental data, and demonstrating that NbTaTiZrHf RHEA exhibits favorable ductility, while NbTaTiZrMo RHEA and NbTaTiZrW RHEA have lower ductility [5,31,35].

The yield strengths of material were calculated by formula (6), which can be further used to analyze the ductility of NbTaTiZrX RHEAs.

$$\sigma_y = \frac{H_v}{3} \quad (6)$$

From Table 4, it is obvious to notice that the calculated yield strength is slightly higher than the experimental yield strength of the alloy. The measured yield strength of NbTaTiZrMo RHEA is 1390 MPa [35], while the yield strength calculated using Vickers hardness is 1630 MPa, which is approximately 17% higher than the measured value. Despite the

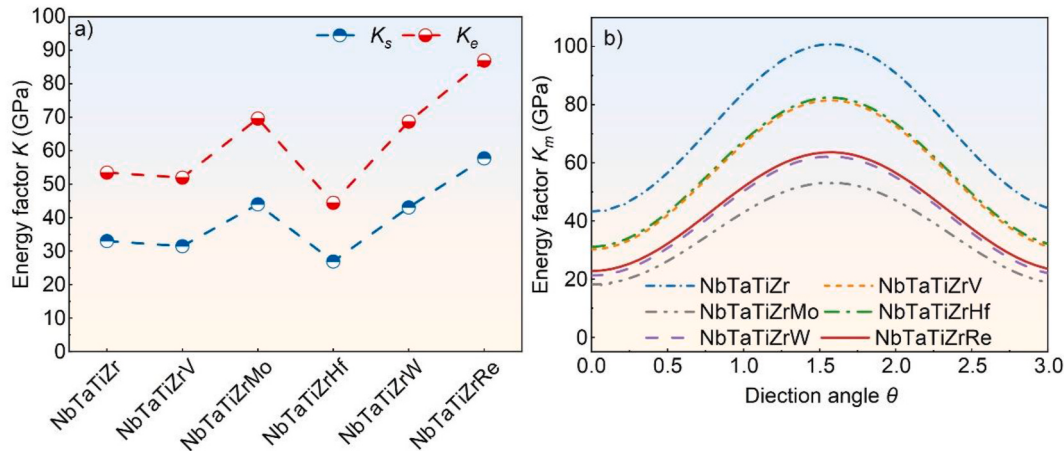


Fig. 5. Energy factors of NbTaTiZrX RHEAs (X = V, Mo, Hf, W, and Re) calculated by SQS method.
a) screw dislocation (K_s) and edge dislocation (K_e); b) mixed dislocation (K_m).

overestimation of yield hardness, the trend of the calculated results is consistent with that of the experiment. Hf-alloying significantly reduces the yield strength of RHEAs, and weakens their resistance to plastic deformation. Nevertheless, the alloying of Mo, W and Re markedly increases the yield strength of RHEAs and thus enhances their resistance to plastic deformation. Notably, by using SQS method, the calculated yield strength of RHEAs exceeds 1 GPa, and NbTaTiZrRe RHEA exceeds 2 GPa, which is significantly higher than the currently studied HEAs. Therefore, it is necessary to conduct systematic research on the mechanical properties of NbTaTiZrRe RHEA.

Deviations in the arrangement of atoms in the crystal from the ideal periodic structure lead to the formation of dislocations, which can affect the material's mechanical properties [46]. The energy factor K can be utilized to assess the dislocation nucleation propensity of materials. Based on formulas (7) - (9), the screw dislocation (K_s), edge dislocation (K_e), and mixed dislocation (K_m) of NbTaTiZrX RHEAs were calculated, as shown in Fig. 5. Where, θ denotes the direction angle of the Burgers vector and dislocation line.

$$K_s = \left[\frac{C_{44}(C_{11} - C_{12})}{2} \right]^{\frac{1}{2}} \quad (7)$$

$$K_e = (C_{11} + C_{12}) \left[\frac{C_{44}(C_{11} - C_{12})}{C_{11}(C_{11} + C_{12} + 2C_{44})} \right]^{\frac{1}{2}} \quad (8)$$

$$K_m = K_e \sin^2 \theta + K_s \cos^2 \theta \quad (9)$$

As shown in Fig. 5, the dislocation nucleation propensity follows the order of $K_{\text{NbTaTiZrRe}} > K_{\text{NbTaTiZrW}} > K_{\text{NbTaTiZrMo}} > K_{\text{NbTaTiZr}} > K_{\text{NbTaTiZrV}} > K_{\text{NbTaTiZrHf}}$, with NbTaTiZrHf RHEA exhibiting notably lower propensity compared to NbTaTiZr RHEA, and even lower than NbTaTiZrMo. This suggests that the nucleation of dislocations is more tendency in NbTaTiZrHf RHEA, while less likely in NbTaTiZrRe RHEA. In addition, screw dislocations ($\theta = 0$) have a smaller energy factor, making them more prone to nucleate compared to edge dislocations ($\theta = \pi/2$). And in perfect crystals, the presence of screw dislocations facilitates deformation. At the same time, it was found in the experiment that more severe lattice distortion is also conducive to promoting the formation of dislocations, increasing the resistance to dislocation movement [41]. Therefore, the addition of Hf element with the maximum radius results in better RHEA plastic deformation.

3.3. Electronic properties

The electronic properties and atomic bonding properties of materials are considerable indicators that influence macroscopic mechanical properties [47,48]. Thus, this study calculated the Total Density of States (TDOS) of NbTaTiZrX RHEAs as shown in Fig. 6 and the Density of States (DOS) for each atom as shown in Fig. 7. As can be seen from Fig. 6, there is no significant difference in the predicted total density of states of NbTaTiZrX RHEAs, indicating a stable phase structure without any phase transition after alloying. Furthermore, the TDOS and DOS of NbTaTiZrX RHEAs at the Fermi level are non-zero, indicating that they have metallic properties. According to Fig. 7, the DOS near the Fermi

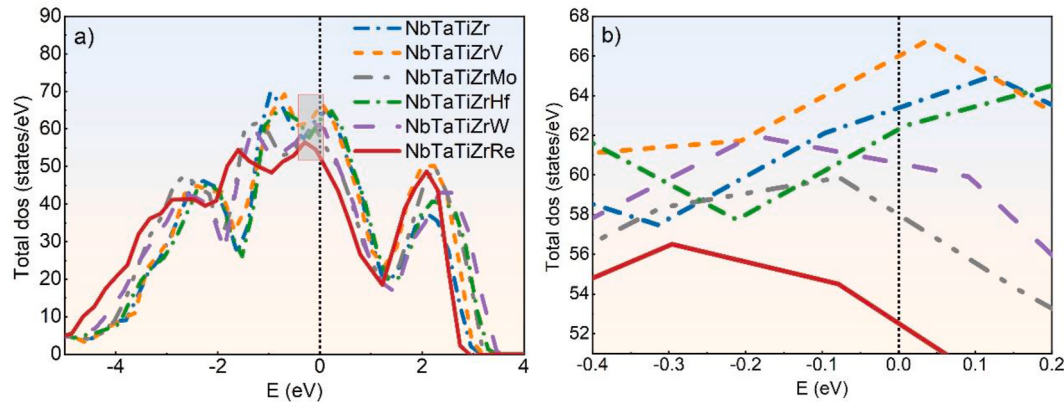


Fig. 6. a) Total density of states for NbTaTiZrX RHEAs (X = V, Mo, Hf, W, and Re) calculated by SQS method. b) Total density of states image taken from the region marked by box in a).

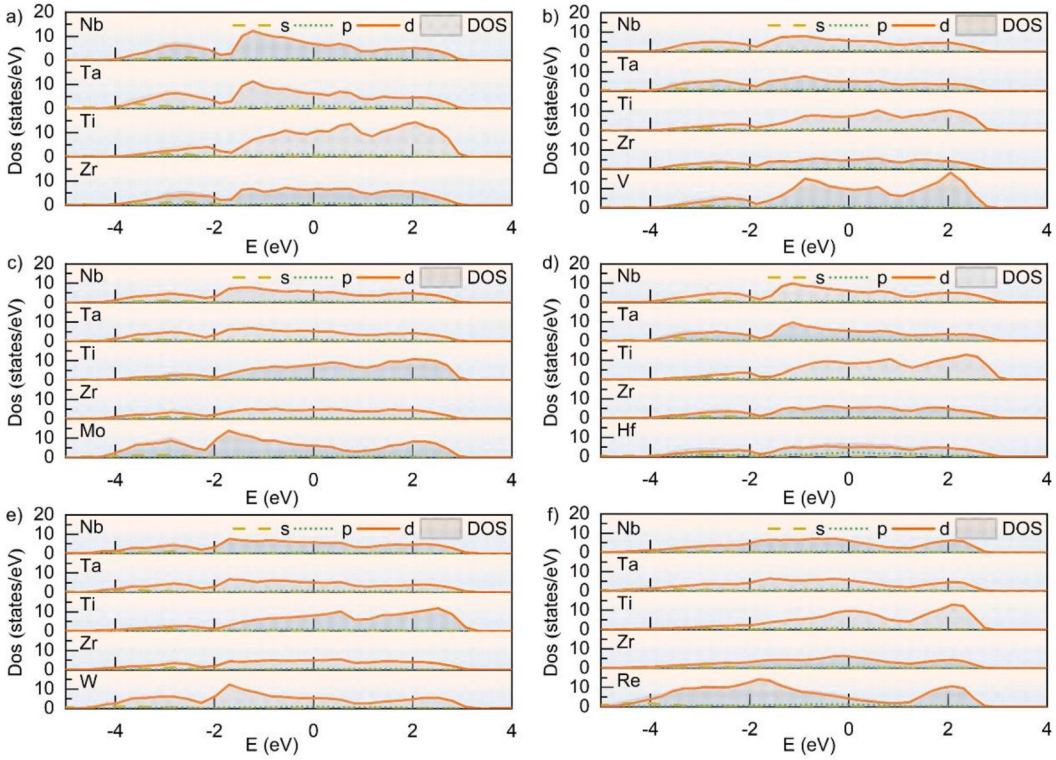


Fig. 7. Density of states for each atom in NbTaTiZrX RHEAs.
a) NbTaTiZr; b) NbTaTiZrV; c) NbTaTiZrMo; d) NbTaTiZrHf; e) NbTaTiZrW; f) NbTaTiZrRe.

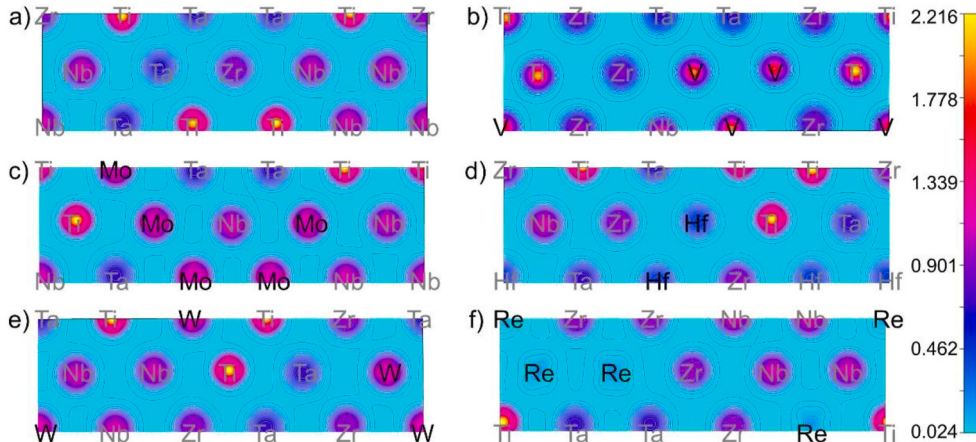


Fig. 8. Charge density contour of NbTaTiZrX RHEAs along the crystal plane (1 1 0).
a) NbTaTiZr; b) NbTaTiZrV; c) NbTaTiZrMo; d) NbTaTiZrHf; e) NbTaTiZrW; f) NbTaTiZrRe.

energy level is primarily contributed by the 3 d orbitals of each refractory element atoms, with an obvious hybridization between them. Additionally, the total density of states of NbTaTiZrRe RHEA is significantly smaller than that of other RHEAs, indicating its weaker metallic properties. The pseudogap refers to the energy difference between two prominent peaks near Fermi level. The wider the pseudogap, the more covalent the material. Fig. 6 reveals that the alloying of Hf and V causes the pseudogap width of RHEAs to sharply decrease, while alloying of Mo, W and Re can significantly increase the width of the pseudogap. This indicates that alloying of Hf and V reduce the number of covalent bonds in RHEAs, resulting in NbTaTiZrHf and NbTaTiZrV RHEAs possessing good ductility. On the other hand, alloying of Mo, W and Re increases the number of covalent bonds, leading to lower ductility of NbTaTiZrMo, NbTaTiZrW and NbTaTiZrRe RHEAs.

Fig. 8 illustrates the charge density contour of NbTaTiZrX RHEAs along the crystal plane (1 1 0). The charge density distribution indicates the presence of overlap in the electron cloud, allowing an intuitive observation of the type of atomic bonding. As shown in the figure, the overlap of RHEAs electron clouds after alloying of Hf and V is significantly reduced, indicating the formation of Hf-Hf and V-V strong metallic bonds, similar to the Zr-Zr strong metallic bonds in NbMo-TaWZr [49], which is consistent with their good ductility. On the contrary, the alloying of Mo, W and Re significantly reduces the strong metal binding in RHEAs. Especially, after Re-alloying, the electron cloud overlaps more around the Re atom and has obvious directionality, while the interaction between electrons is significantly weakened, confirming the formation of covalent bonds. This also supports that NbTaTiZrRe RHEA has high yield strength and hardness, and provides theoretical

support for its future experimental synthesis and preparation.

In our next stage of RHEAs research, we will carry out the experimental work further to verify the above-mentioned calculation results of the exploration of new RHEAs, and in order to clarify the theoretical reason of their excellent mechanical properties, accelerate the exploration and application process of new RHEAs, even provide more suitable metallic materials for aerospace and other applications.

4. Conclusions

The effect of elemental alloying on the mechanical and electronic properties of NbTaTiZrX (X = V, Mo, Hf, W and Re) high-entropy alloys are studied through first-principles calculations. The VEC and other parameters indicate that NbTaTiZrX RHEAs are high-entropy alloys with BCC structure. After optimizing the structure, the calculated XRD of NbTaTiZrX RHEAs is consistent with the experiment results. The alloying of Re with the smallest radius and Hf with the largest radius give RHEAs the smallest and the largest lattice constant, respectively. Alloying of Mo, W and Re with high elastic modulus can improve the deformation resistance of RHEAs and reduce their ductility. Among them, Re-alloying has the most significant strengthening effect, with hardness and yield strength values of 7.03 GPa and 2.32 GPa, respectively, which are markedly higher than those of the high-entropy alloys currently studied. However, NbTaTiZrHf RHEA exhibit excellent plastic properties and their screw dislocations are more prone to nucleate. The electronic properties reveal that Hf-alloying reduces the pseudo band gap and enhances metallicity. Additionally, the formation of Hf–Hf metallic bonds effectively enhances the metallic ductility of NbTaTiZrHf RHEA. The calculated results agree with the previously reported experiments, which also provides guidance for further experimental and practical researches.

Declaration of competing interest

The authors declare that they have no known competing financial interests or personal relationships that could have appeared to influence the work reported in this paper.

Acknowledgements

This work was financially supported by the National Natural Science Foundation of China (NSFC) under grant no. 52061035, Young Leading Talent of “Grassland Talents” Project of Inner Mongolia Autonomous Region (no. QNLJ012010), Program for Innovative Research Team in Universities of Inner Mongolia Autonomous Region (no. NMGIRT2211), Inner Mongolia University of Technology Key Discipline Team Project of Materials Science (no. ZD202012).

Appendix A. Supplementary data

Supplementary data to this article can be found online at <https://doi.org/10.1016/j.jmrt.2024.05.253>.

References

- [1] Yeh JW, Chen SK, Lin SJ, Gan JY, Chin TS, Shun TT, Tsau CH, Chang SY. Nanostructured high-entropy alloys with multiple principal elements: novel alloy design concepts and outcomes. *Adv Eng Mater* 2004;6(5):299–303. <https://doi.org/10.1002/adem.200300567>.
- [2] Tracy CL, Park S, Rittman DR, Zinkle SJ, Bei H, Lang M, Ewing RC, Mao WL. High pressure synthesis of a hexagonal close-packed phase of the high-entropy alloy CrMnFeCoNi. *Nat Commun* 2017;8:15634. <https://doi.org/10.1038/ncomms15634>.
- [3] Xiong W, Guo AXY, Zhan S, Liu CT, Cao SC. Refractory high-entropy alloys: a focused review of preparation methods and properties. *J Mater Sci Technol* 2023; 142:196–215. <https://doi.org/10.1016/j.jmst.2022.08.046>.
- [4] Senkov ON, Wilks GB, Scott JM, Miracle DB. Mechanical properties of Nb₂₅Mo₂₅Ta₂₅W₂₅ and V₂₀Nb₂₀Mo₂₀Ta₂₀W₂₀ refractory high entropy alloys. *Intermetallics* 2011;19(5):698–706. <https://doi.org/10.1016/j.intermet.2011.01.004>.
- [5] Fan XJ, Qu RT, Zhang ZF. Remarkably high fracture toughness of HfNbTaTiZr refractory high-entropy alloy. *J Mater Sci Technol* 2022;123:70–7. <https://doi.org/10.1016/j.jmst.2022.01.017>.
- [6] Juan CC, Tsai MH, Tsai CW, Lin CM, Wang WR, Yang CC, Chen SK, Lin SJ, Yeh JW. Enhanced mechanical properties of HfMoTaTiZr and HfMoNbTaTiZr refractory high-entropy alloys. *Intermetallics* 2015;62:76–83. <https://doi.org/10.1016/j.intermet.2015.03.013>.
- [7] Zhou YK, Zeng S, Li H, Zhang HW, Zhang HF, Zhu ZW. A design of Zr-rich body-centered cubic structured refractory complex concentrated alloy with outstanding tensile strength and ductility. *Mater Sci Eng, A* 2023;874:145091. <https://doi.org/10.1016/j.msea.2023.145091>.
- [8] Li TX, Wang SD, Fan WX, Lu YP, Wang TM, Li TJ, Liaw PK. CALPHAD-aided design for superior thermal stability and mechanical behavior in a TiZrHfNb refractory high-entropy alloy. *Acta Mater* 2023;246:118728. <https://doi.org/10.1016/j.actamat.2023.118728>.
- [9] Li H, Zeng S, Zhou YK, Li HL, Zhang HW, Zhang HF, Zhu ZW. High tensile strength and superelasticity of directionally solidified Ti₃₀Ni₃₀Fe₁₀Hf₁₀Nb₂₀ eutectic high entropy alloy. *Acta Metall. Sin-Engl.* 2022;35(10):1583–90. <https://doi.org/10.1007/s40195-022-01434-2>.
- [10] Lei ZF, Liu XJ, Wu Y, Wang H, Jiang SH, Wang SD, Hui XD, Wu YD, Gault B, Kontis P, Raabe D, Gu L, Zhang QH, Chen HW, Wang HT, Liu JB, An K, Zeng QS, Nieh TG, Lu ZP. Enhanced strength and ductility in a high-entropy alloy via ordered oxygen complexes. *Nature* 2018;563(7732):546–50.
- [11] Nguyen VT, Qian M, Shi Z, Song T, Huang L, Zou J. A novel quaternary equiatomic Ti-Zr-Nb-Ta medium entropy alloy (MEA). *Intermetallics* 2018;101:39–43. <https://doi.org/10.1016/j.intermet.2018.07.008>.
- [12] Guo NN, Wang L, Luo LS, Li XZ, Su YQ, Guo JJ, Fu HZ. Microstructure and mechanical properties of refractory MoNbHfZrTi high-entropy alloy. *Mater Des* 2015;81:87–94. <https://doi.org/10.1016/j.matdes.2015.05.019>.
- [13] Todai M, Nagase T, Hori T, Matsugaki A, Sekita A, Nakano T. Novel TiNbTaZrMo high-entropy alloys for metallic biomaterials. *Scripta Mater* 2017;129:65–8. <https://doi.org/10.1016/j.scriptamat.2016.10.028>.
- [14] Yang W, Liu Y, Pang S, Liaw PK, Zhang T. Bio-corrosion behavior and in vitro biocompatibility of equimolar TiZrHfNbTa high-entropy alloy. *Intermetallics* 2020; 124:106845. <https://doi.org/10.1016/j.intermet.2020.106845>.
- [15] Bhandari U, Ghadimi H, Zhang CY, Gao F, Yang SZ, Guo SM. Computational exploration of biomedical HfNbTaTiZr and Hf_{0.5}Nb_{0.5}Ta_{0.5}Ti_{1.5}Zr refractory high-entropy alloys. *Mater Res Express* 2021;8(9):096534. <https://doi.org/10.1088/2053-1591/ac1d65>.
- [16] Gao Y, Qiao LJ, Wu DT, Zhang YG, Zou Y. First principle calculation of the effect of Cr, Ti content on the properties of VMoNbTaWM_x (M = Cr, Ti) refractory high entropy alloy. *Vacuum* 2020;179:109459. <https://doi.org/10.1016/j.vacuum.2020.109459>.
- [17] Qiao LJ, Liu Y, Gao Y, Bi JQ, Li YH, Liu C, Gao J, Wang WL, Qian Z. First-principles prediction, fabrication and characterization of (Hf_{0.2}Nb_{0.2}Ta_{0.2}Ti_{0.2}Zr_{0.2})B₂ high-entropy borides. *Ceram Int* 2022;48(12):17234–45.
- [18] Wei SH, Ferreira LG, Bernard JE, Zunger A. Electronic properties of random alloys: Special quasirandom structures. *Phys Rev B* 1990;42(15):9622–49. <https://doi.org/10.1103/PhysRevB.42.9622>.
- [19] Walle AVD, Tiwary P, Jong MD, Olmsted DL, Asta M, Dick A, Shin D, Wang Y, Chen LQ, Liu ZK. Efficient stochastic generation of special quasirandom structures. *Calphad* 2013;42:13–8. <https://doi.org/10.1016/j.calphad.2013.06.006>.
- [20] Walle AVD, Asta M, Ceder G. The alloy theoretic automated toolkit: A user guide. *Calphad* 2002;26(4):539–53. [https://doi.org/10.1016/S0364-5916\(02\)80006-2](https://doi.org/10.1016/S0364-5916(02)80006-2).
- [21] Bellalche L, Vanderbilt D. Virtual crystal approximation revisited: Application to dielectric and piezoelectric properties of perovskites. *Phys Rev B* 2000;61(12): 7877–82. <https://doi.org/10.1103/PhysRevB.61.7877>.
- [22] Kresse G, Furthmüller J. Efficient iterative schemes for ab initio total-energy calculations using a plane-wave basis set. *Phys Rev B Condens Matter* 1996;54(16): 11169–86. <https://doi.org/10.1103/PhysRevB.54.11169>.
- [23] Hohenberg P, Kohn W. Inhomogeneous electron gas. *Phys Rev* 1964;136(3B): B864–71. <https://doi.org/10.1103/PhysRev.136.B864>.
- [24] Perdew JP, Burke K, Ernzerhof M. Generalized gradient approximation made simple. *Phys Rev Lett* 1996;77(18):3865–8. <https://doi.org/10.1103/PhysRevLett.77.3865>.
- [25] Blöchl PE. Projector augmented-wave method. *Phys Rev B Condens Matter* 1994; 50(24):17953–79. <https://doi.org/10.1103/PhysRevB.50.17953>.
- [26] Wang V, Xu N, Liu JC, Tang G, Geng WT. VASPKIT: A user-friendly interface facilitating high-throughput computing and analysis using VASP code. *Comput Phys Commun* 2021;267:108033. <https://doi.org/10.1016/j.cpc.2021.108033>.
- [27] Zhang Y, Zhou YJ, Lin JP, Chen GL, Liaw PK. Solid-solution phase formation rules for multi-component alloys. *Adv Eng Mater* 2008;10(6):534–8. <https://doi.org/10.1002/adem.200700240>.
- [28] Yang X, Zhang Y. Prediction of high-entropy stabilized solid-solution in multi-component alloys. *Mater Chem Phys* 2012;132(2–3):233–8. <https://doi.org/10.1016/j.matchemphys.2011.11.021>.
- [29] Guo S, Ng C, Lu J, Liu CT. Effect of valence electron concentration on stability of fcc or bcc phase in high entropy alloys. *J Appl Phys* 2011;109(10):103505. <https://doi.org/10.1063/1.3587228>.
- [30] Pugh SF. XCII. Relations between the elastic moduli and the plastic properties of polycrystalline pure metals. *Lond. Edinb. Dublin philos. mag. j. sci.* 1954;45(367): 823–43. <https://doi.org/10.1080/14786440808520496>.
- [31] Nagase T, Mizuuchi K, Nakano T. Solidification microstructures of the ingots obtained by arc melting and cold crucible levitation melting in TiNbTaZr medium-

- entropy alloy and TiNbTaZrX (X= V, Mo, W) high-entropy alloys. *Entropy* 2019;21(5):483. <https://doi.org/10.3390/e21050483>.
- [32] Senkov ON, Scotta JM, Senkova SV, Miraclea DB, Woodwarda CF. Microstructure and room temperature properties of a high-entropy TaNbHfZrTi alloy. *J Alloys Compd* 2011;509:6043–8. <https://doi.org/10.1016/j.jallcom.2011.02.171>.
- [33] Denton AR, Ashcroft NW. Vegard's law. *Phys. Rev. A* 1991;43:3161–4. <https://doi.org/10.1103/PhysRevA.43.3161>.
- [34] Juan CC, Tseng KK, Hsu WL, Tsai MH, Tsai CW, Lin CM, Chen SK, Lin SJ, Yeh JW. Solution strengthening of ductile refractory HfMo_xNbTaTiZr high-entropy alloys. *Mater Lett* 2016;175:284–7. <https://doi.org/10.1016/j.matlet.2016.03.133>.
- [35] Wang SP, Xu J. TiZrNbTaMo high-entropy alloy designed for orthopedic implants: as-cast microstructure and mechanical properties. *Mater Sci Eng C* 2017;73:80–9. <https://doi.org/10.1016/j.msec.2016.12.057>.
- [36] Tong YG, Bai LH, Liang XB, Hua MY, Liu J, Li YJ, Zhang J, Hu YL. Mechanical performance of (NbTaW)_{1-x}Mo_x ($x = 0, 0.05, 0.15, 0.25$) refractory high entropy alloys: Perspective from experiments and first principles calculations. *J Alloys Compd* 2021;873:159740. <https://doi.org/10.1016/j.jallcom.2021.159740>.
- [37] Hill R. The Elastic Behaviour of a crystalline aggregate. *Proc Phys Soc Sect A* 1952; 65:349. <https://doi.org/10.1088/0370-1298/65/5/307>.
- [38] Zýka J, Málek J, Veselý J, Lukáč F, Čížek J, Kuríplach J, Melikhova O. Microstructure and room temperature mechanical properties of different 3 and 4 element medium entropy alloys from HfNbTaTiZr system. *Entropy* 2019;21(2):114. <https://doi.org/10.3390/e21020114>.
- [39] Wang SP, Xu J. (TiZrNbTa)-Mo high-entropy alloys: Dependence of microstructure and mechanical properties on Mo concentration and modeling of solid solution strengthening. *Intermetallics* 2018;95:59–72. <https://doi.org/10.1016/j.intermet.2018.01.017>.
- [40] He Q, Yoshida SH, Yasuda H, Tsuji N. Effect of elemental combination on microstructure and mechanical properties of quaternary refractory medium Entropy Alloys. *Mater Trans* 2022;61(4):577–86. <https://doi.org/10.1016/j.msea.2012.07.003>.
- [41] Wu RJ, Xie ZC, Xu SZ, Su YQ, Yao XH, Beyerlein IJ. Effects of lattice distortion and chemical short-range order on the mechanisms of deformation in medium entropy alloy CoCrNi. *Acta Mater* 2020;199:352–69. <https://doi.org/10.1016/actamat.2020.08.0441>.
- [42] Zhao EJ. Theoretical study on the mechanical and electronic properties of the transition metal borides, carbides and nitrides. Changchun: Changchun Institute of Applied Chemistry Chinese Academy of Sciences; 2007.
- [43] Fu HZ, Li DH, Peng F, Cao T, Cheng XL. Ab initio calculations of elastic constants and thermodynamic properties of NiAl under high pressures. *Comput Mater Sci* 2008;44(2):774–8. <https://doi.org/10.1016/j.intermet.2009.12.005>.
- [44] Mo JY, Wan YX, Zhang ZB, Wang X, Li XQ, Shen BL, Liang XB. First-principle prediction of structural and mechanical properties in NbMoTaWRex refractory high-entropy alloys with experimental validation. *Rare Met* 2022;41(10):3343–50. <https://doi.org/10.1007/s12598-022-02054-6>.
- [45] Ji GY, Zhou ZK, Meng FC, Yang X, Sheng RX, Qiao JB, Liaw PK, Li M, Jiang L, Chen SY, Tong Y. Effect of Zr addition on the local structure and mechanical properties of Ti-Ta-Nb-Zr refractory high-entropy alloys. *J Mater Res Technol* 2022;19:4428–38. <https://doi.org/10.1016/j.jmrt.2022.06.160>.
- [46] Foreman AJE. Dislocation energies in anisotropic crystals. *Acta Metall* 1955;3: 322–30. [https://doi.org/10.1016/0001-6160\(55\)90036-5](https://doi.org/10.1016/0001-6160(55)90036-5).
- [47] Koval NE, Juaristi JI, Díez Muñoz R, Alducin M. Elastic properties of the TiZrNbTaMo multi-principal element alloy studied from first principles. *Intermetallics* 2019;106:130–40. <https://doi.org/10.1016/j.intermet.2018.12.014>.
- [48] Zhao Q, Li J, Fang Q, Feng H. Effect of Al solute concentration on mechanical properties of Al_xFeCuCrNi high-entropy alloys: A first-principles study. *Phys B Condens Matter* 2019;566:30–7. <https://doi.org/10.1016/j.physb.2019.04.025>.
- [49] Hu YL, Bai YG, Tong YG, Deng DY, Liang XB, Zhang J, Li YJ, Chen YX. First-principle calculation investigation of NbMoTaW based refractory high entropy alloys. *J Alloys Compd* 2020;827:153963. <https://doi.org/10.1016/j.jallcom.2020.153963>.